REGULAR PAPER

Computational complexity reduction techniques for real-time and high-resolution medical ultrasound imaging using the beam-space Capon method

Shigeaki Okumura[1]*, Hirofumi Taki[2], and Toru Sato[1]

[1]*Graduate School of Informatics, Kyoto University, Kyoto 606-8501, Japan*
[2]*Graduate School of Biomedical Engineering, Tohoku University, Sendai 980-8579, Japan*

*E-mail: sokumura@sato-lab.0t0.jp

The beam-space (BS) Capon method is an adaptive beamforming technique that reduces computational complexity. However, the complexity is not low enough for real-time imaging. Reducing the number of time-delay and transformation processes from element-space to BS signal processing is required. We propose a technique that replaces the time-delay processes by the multiplication of steering vectors and covariance matrices. In addition, we propose a compensation technique for estimating the intensity accurately. In an experimental study using a 2.0 MHz transmission frequency on a 15 × 10.4 mm^2 region of interest, the first side-lobe level, the −6 dB beam width, the intensity's estimation error, and the calculation time of the conventional method were −15 dB, 0.70 mm, 3.2 dB, and 656 ms. Those of the proposed method were −17 dB, 0.36 mm, 1.6 dB, and 81 ms, respectively. Using our method on three CPUs achieves imaging of 37 frames/s. © 2016 The Japan Society of Applied Physics

1. Introduction

Medical ultrasound imaging is a real-time, noninvasive and low-cost test for medical diagnosis.[1–6] Improvements in resolution and contrast in medical ultrasound imaging are strongly desired because they facilitate accurate medical diagnosis.[7–10] The delay-and-sum (DAS) beamforming technique, a basic nonadaptive beamforming strategy, has been employed in commercial medical ultrasound devices. However, the resolution is determined by the probe's aperture size. Recently, several adaptive beamforming techniques that improve spatial resolution have been proposed to improve lateral resolution[11–18] and axial resolution.[19–23] However, for lateral resolution improvement, large computational complexity has prevented implementation into commercial ultrasound devices.[11,12]

The Capon method is an adaptive beamforming technique.[24] In the method, the optimal weighting vector is calculated by minimizing the output power under a constraint condition that maintains the response at a particular measurement point. The original Capon method for ultrasound imaging is based on element-space (ES) signal processing.[14–16] ES signal processing requires the inversion of large matrices, which severely increases the complexity. To reduce the complexity associated with calculating inverse matrices, the beam-space (BS) Capon method has been reported.[11–13] The method uses a few orthogonal beams to reduce the matrix size. The BS Capon method reduces complexity compared with the original ES Capon method. However, further reduction is required for real-time imaging.

Because ultrasound imaging typically employs wide-band signals, both ES and BS Capon methods employ a large number of time-delay processes to create focal points in the region of interest (ROI) and to estimate the covariance matrix. In addition, compared with the ES Capon method, the BS Capon method requires an additional calculation associated with the transformation from ES signal processing to BS signal processing.[11–13] To achieve real-time imaging, reductions are required in the number of the above-mentioned processes.

When the time-delay value to generate a focal point is small, the time-delay process can be approximated by multiplying a steering vector with a covariance matrix.[12] Thus, we propose a method that reduces the number of processes by using this approximation.

Additionally, an accurate estimation of the intensity is required in medical ultrasound imaging. The spatial averaging (SA) technique is widely employed to stabilize the estimation of the intensity when using the Capon method.[12,13,19–23,25] A smaller size of SA achieves higher resolution and low stability, whereas a larger size of SA achieves lower resolution and high stability. Therefore, we first employ a smaller size of SA for high-resolution imaging and estimate the position at which the target should exist. Next, we use a larger size of SA to compensate the intensity. In this work, to evaluate the proposed method, we conducted a numerical simulation and an experiment.

2. Materials and methods

2.1 Original BS Capon method

We introduce the original BS Capon method for medical ultrasound imaging that is the basis of the proposed method.[11] The BS method first multiplies the Butler matrix, **B**, to the signal vector after a time-delay process, $\mathbf{y}(t)$, to form orthogonal beams. Because the spatial energy distribution of transmitted ultrasound is determined by the position of the transmitted beam, we can select a few useful beams that contain signals returned from the desired direction.[11–13] When we use an M-element linear array with the element pitch of a half-wavelength at the center frequency, the received signal vector in the BS, $\mathbf{y}_{\mathrm{BS}}(t)$, is given by

$$\mathbf{y}_{\mathrm{BS}}(t) = \mathbf{B}\mathbf{y}(t), \tag{1}$$

$$\mathbf{B} = [\mathbf{b}_{-(L-1)/2} \cdots \mathbf{b}_0 \cdots \mathbf{b}_{(L-1)/2}]^{\mathrm{T}}, \tag{2}$$

$$[\mathbf{b}_q]_p = \exp(j2\pi pq/M)/\sqrt{M}, \tag{3}$$

where L is the number of the selected beams, p, q are the element indices of the matrix, and $[\cdots]^{\mathrm{T}}$ denotes the transpose. In this study, we assume M is an even number and use $L = 3$ to follow previous studies.[11–13]

The Capon method assumes that the desired signal has no correlations with off-axis signals. To suppress the correlation, the SA technique is widely applied. The covariance matrix using SA, $\mathbf{R}_{\mathrm{A}}$, is given by

$$[\mathbf{R}_A]_{p,q} = \sum_{n=1}^{L_{ave}} y_{n+p-1}(t)y_{n+q-1}^*(t)/L_{ave}, \quad (4)$$

where $y_m(t)$ is the received signal at the m-th element, L_{ave} is the size of SA, and the size of $\mathbf{R}_A$ is $L_{sub} = M - L_{ave} + 1$. In this study, we call L_{sub} the "subarray size".

The BS Capon method then computes the optimal weighting vector by solving

$$\min_{\mathbf{W}_{BS}}(P_{out} = \mathbf{W}_{BS}^H \mathbf{R}_{ABS} \mathbf{W}_{BS}/2) \text{ subject to } \mathbf{W}_{BS}\mathbf{C} = 1, \quad (5)$$

$$\mathbf{R}_{ABS} = \mathbf{B}_S \mathbf{R}_A \mathbf{B}_S^H, \quad (6)$$

$$\mathbf{C} = \mathbf{B}_S[1\cdots 1]^T, \quad (7)$$

where P_{out} is the output power of the BS Capon, $\mathbf{W}_{BS}$ is the weighting vector, $[\cdots]^H$ denotes the Hermitian transpose, $\mathbf{B}_s$ is the Butler matrix for the subarray, $\mathbf{C}$ is the steering vector, and $\mathbf{R}_{ABS}$ is the covariance matrix in the BS. The output power is expressed as

$$P_{out} = 1/\{\mathbf{C}^H[\mathbf{R}_{ABS} + \eta\mathbf{I}]^{-1}\mathbf{C}\}, \quad (8)$$

where η is the diagonal loading factor used to stabilize the estimated intensity and $\mathbf{I}$ is the identity matrix. The diagonal loading factor determines the sensitivity of the Capon method. When we use a large diagonal loading factor, the output power approaches that of the DAS technique. Conversely, a small diagonal loading factor results in a high-resolution image and a large estimation error of the output power.

Compared with the ES Capon method, the BS method reduces the computational complexity associated with the inversion of the covariance matrix. However, additional reduction of complexity is desired for clinical use. In addition, both accurate estimation of intensity and high-resolution imaging are required. We thus employ the following three steps.

2.2 Computational complexity reduction using a steering vector

To reduce the computational complexity, we replace the time-delay process by the multiplication of a steering vector with an estimated covariance matrix. We first divide the ROI into sub-ROIs, as shown in Fig. 1. The output powers at the measurement points in a sub-ROI are estimated using a covariance matrix at the center of the sub-ROI with steering vectors. That is, we approximate the time-delay process that is focused on the measurement point with a steering vector
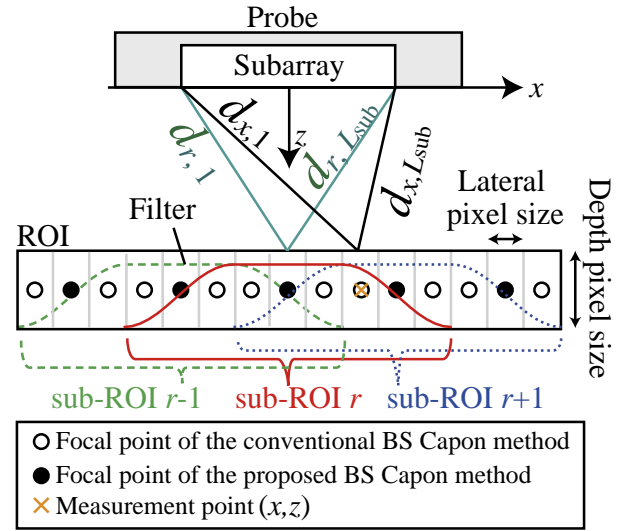

Fig. 1. (Color online) Schematic illustration of proposed method.

and a time-delay process that is focused at the center of the sub-ROI.

The output power at (x, z) in sub-ROI r, $P_{outr}(x, z)$, is estimated by the proposed BS Capon method using the steering vector $\mathbf{C}_r'(x, z)$:

$$P_{outr}(x, z) = 1/\{\mathbf{C}_r'(x, z)^H[\mathbf{R}_{ABS}(x_r, z) + \eta\mathbf{I}]^{-1}\mathbf{C}_r'(x, z)\}, \quad (9)$$

$$\mathbf{C}_r'(x, z) = \mathbf{B}[\exp(j\theta_1)\cdots\exp(j\theta_{L_{sub}})]^T, \quad (10)$$

$$\theta_m = \omega_c(d_{r,m} - d_{x,m})/c, \quad (11)$$

where $\mathbf{R}_{ABS}(x_r, z)$ is the covariance matrix when the beam is focused at the center of the sub-ROI (x_r, z), r is the sub-ROI index, c is the speed of sound, ω_c is the center angular frequency, and $d_{r,m}$ and $d_{x,m}$ are the distances from the m-th element in the subarray to the focal points (x_r, z) and (x, z), respectively. When we reduce the number of time-delay processes, the transformation from ES signal processing to BS signal processing is also simplified because we can reuse the BS covariance matrix in the sub-ROI.

Because the steering vector $\mathbf{C}_r'$ compensates for the phase rotation at the center frequency, the large distance from the focal point to the measurement point $d_{r,m} - d_{x,m}$ should deteriorate the image quality of the proposed method. As shown in Fig. 1, we mitigate the deterioration with a filter, $w_r(x)$, that amplifies the output power calculated at the center of the sub-ROI:

$$w_r(x) = \begin{cases} \{\sin[3\pi(x - x_r)/x_s + \pi] + 1\}/4 & \text{for } x_r - x_s/2 \le x \le x_r - x_s/6 \\ 0.5 & \text{for } x_r - x_s/6 \le x \le x_r + x_s/6 \\ \{\sin[3\pi(x - x_r)/x_s] + 1\}/4 & \text{for } x_r + x_s/6 \le x \le x_r + x_s/2 \\ 0 & \text{for else} \end{cases}, \quad (12)$$

where x_s is the sub-ROI size and the interval of x_r is $x_s/3$. In this study, we set the distance threshold, $x_s/3$, to be is almost equal to the main beam width.

The output power with the filter, $P_{out}'(x, z)$, is given by

$$P_{out}'(x, z) = \sum_{r=1}^{n_R} w_r(x)P_{outr}(x, z), \quad (13)$$

where n_R is the number of sub-ROIs.

2.3 Sensing target position with peak detection and refocusing

Since the large distance from the focal point to the measurement point causes false images, we must make new focal points and recalculate the intensity at positions nearer to where the targets exists. To select the points, we first search the peaks in $P_{out}'(x, z)$ because the target is most likely to exist at a position where the estimated intensity is high. In this

study, we select peaks that satisfy either of the following two conditions:

$$\frac{P'_{\text{out}}(x, z) - P'_{\text{out}}(x - \Delta x, z)}{\Delta x} > \varepsilon \text{ and } \frac{P'_{\text{out}}(x + \Delta x, z) - P'_{\text{out}}(x, z)}{\Delta x} < 0, \quad (14)$$

$$\frac{P'_{\text{out}}(x, z) - P'_{\text{out}}(x - \Delta x, z)}{\Delta x} > 0 \text{ and } \frac{P'_{\text{out}}(x + \Delta x, z) - P'_{\text{out}}(x, z)}{\Delta x} < -\varepsilon, \quad (15)$$

where ε is the threshold for peak detection and Δx is the lateral pixel size.

The false image may appear near the actual target position. Thus, when the lateral distance of adjacent peaks is less than a threshold distance, x_c, we consider the peaks to be originating from a single target and these peaks are classified into the same cluster. After clustering, we designate a focal point at the center of each cluster and recalculate the intensity at $x_l - x_{\text{re}}/2 < x_l < x_l + x_{\text{re}}/2$, where x_l is the center of the cluster l and x_{re} is the lateral length of recalculation. If the peaks appear again in the region of recalculation, the targets are assumed to exist at the peaks' positions.

2.4 Power compensation technique

In the previous step, we estimated the target positon, x_k, accurately. In the next step, we acquire an accurate approximation of the intensity at x_k. When a large SA size is used for the Capon method, the output power approaches the intensity estimated by DAS method.[13,19–23,25] Because the large distance from the focal point to the measurement point also deteriorates the accuracy of intensity estimation, we set focal points at all x_k. Then we calculate the output power using a large SA size, that is, a small subarray size L'_{sub}. Finally, we linearly interpolate the intensity of the measurement points $P'_{\text{out}}(x)$ in the range of $x_k - x_c < x < x_k + x_c$, where we adjust the intensity at the target position to the above-mentioned estimated intensity.

2.5 Simulation settings

To demonstrate the effectiveness of the proposed method, we used a numerical simulation employing the Field II simulation package.[26,27] We used a 96-element probe with a center frequency of 2.0 MHz and a fractional bandwidth of 50% to simulate the experimental setting. The element pitch was half of the wavelength at the center frequency, that is, 0.375 mm. The two scatterers were positioned at depths of 20 and 50 mm with a lateral interval of 1.0 mm. The lateral pixel size Δx was 0.050 mm and threshold ε was 0.02 W/mm, where the intensity was normalized to the highest intensity. The lateral imaging width was from −3.0 to 3.0 mm.

The sub-ROI size, x_s, was 2.25 mm, the length for recalculation, x_{re}, was 0.55 mm, and the length for clustering, x_c, was 0.30 mm. The distance threshold, $x_s/3$, was almost equal to the main-lobe width at the depth of 35 mm. The subarray size for imaging, L_{sub}, and the subarray size for compensation, L'_{sub}, were 64 and 32, respectively, and the diagonal loading factors for imaging, η, and compensation were −60 and −40 dB of the received signal intensity, respectively.

2.6 Experimental settings

We conducted an experimental study to investigate the performance of the proposed method. Figures 2(a) and 2(b) show a photograph and a schematic of the experimental
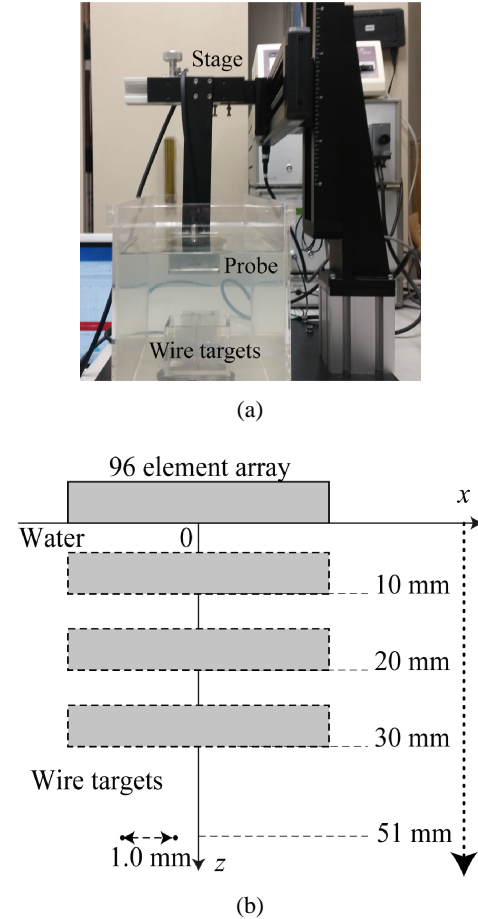

(a)

(b)

Fig. 2. (Color online) (a) Photograph of experimental setup, and (b) schematic illustration of the measurement system with two wire targets in the water tank.

system, respectively. We placed two copper wire targets with a lateral interval of 1.0 mm in a water tank. The diameter of the wire was 0.20 mm. For simplicity, we evaluated the performance of the proposed technique in a two-dimensional (2D) problem. We used a JPR 10-CN (Japan Probe) ultrasound device that can export raw RF data.[28] The sampling frequency was 20 MHz. Because the JPR 10-CN that exports the RF data uses two separate elements to transmit and receive, we employed the synthetic aperture technique to simulate plane wave transmission.[28–31] We changed the target depth by scanning down the probe. Figure 2(b) shows the data-acquisition procedure. The target depths were 21, 31, 41, and 51 mm. The conventional BS Capon method employed a subarray size of 64 and diagonal loading factor of −40 dB to follow the conventional study.[20] The ROI size at each scanning depth was $15 \times 10.4 \text{ mm}^2$. The other parameters are the same as those used in the numerical simulation study.

We evaluated the proposed method using five indicators: the first side-lobe level, the −6 dB beam width, the intensity
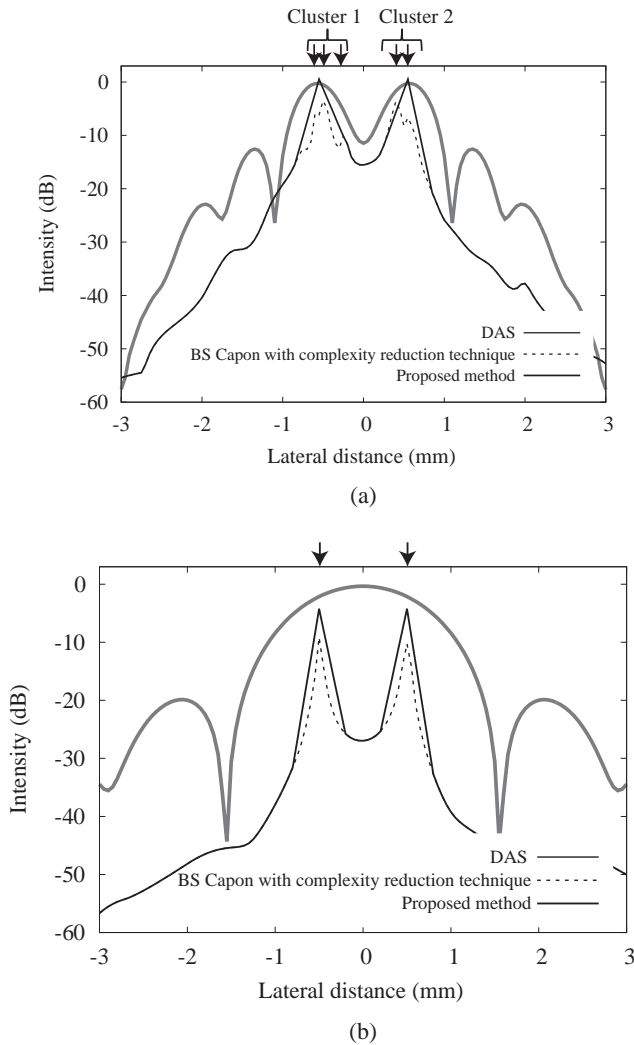
(a)

(b)

Fig. 3. Intensity estimated by DAS method, BS Capon method with complexity reduction, and proposed method at the depths of (a) 20 and (b) 50 mm.

Fig. 4. (Color online) Experimental results of B-mode images of wire targets obtained by (a) the DAS method, (b) the conventional BS Capon, and (c) the proposed BS Capon method. The lateral intervals of the targets were 1.0 mm.

estimation error, the number of operations, and the calculation time. The first side-lobe level was calculated from the intensity at the center of the two wire targets. The −6 dB beam width is the lateral width of the region centered on the target position where the estimated intensity has decreased by less than 6 dB relative to the estimated peak intensity. The intensity estimation error was calculated as the difference between the estimated intensity and the intensity estimated using the DAS method at the target position. We dismissed the running time of loading the experimental data. In the evaluation, we averaged the first side-lobe level, −6 dB beam width, and the intensity estimation error at the each lateral position where the estimated intensity is highest in the ROIs.

3. Simulation and experimental results

3.1 Simulation results

The intensities estimated by the DAS method and the proposed method at the depths of 20 and 50 mm are shown in Figs. 3(a) and 3(b). The dotted lines shown in Fig. 3 are the estimated intensity, P'_{out}, obtained by the proposed BS Capon method with only the complexity reduction technique. The false images appeared at lateral distances of around −0.50
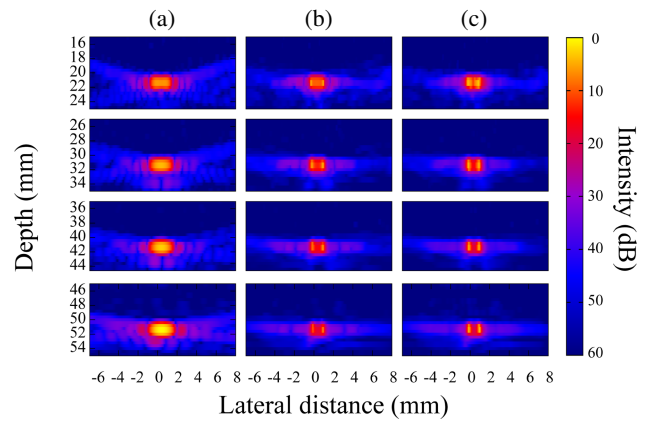
and 0.50 mm. The arrows show the detected peaks in output power P'_{out}.

The solid black line in Fig. 3 shows the output power obtained using both the complexity reduction technique and compensation technique. The numbers of processes associated with the time-delay and the transformation of the conventional method and the proposed method were 121 and 12, respectively. The estimation errors of the proposed method at the target locations are 1.2 and 2.0 dB at depths of 20 and 50 mm, respectively. These results show that the proposed method successfully yielded high-resolution and high-contrast images with accurate intensity estimation and low computational complexity.

3.2 Experimental results

Figure 4 shows the images acquired by the three methods: (a) the DAS method, (b) the conventional BS Capon method with a subarray size of 64, and (c) the proposed method. The dynamic range in the figure is 60 dB. Figures 5(a), 5(b), 5(c), and 5(d) are cross-sectional views of Fig. 4 at 21.4, 31.4, 41.4, and 51.4 mm depths, where the B-mode image acquired by the DAS method has maximum intensity. Table I shows the evaluation indicators.

The first side-lobe levels of the DAS method, conventional BS Capon method, and the proposed BS Capon method with the compensation technique were −5.3, −15, and −17 dB, respectively. The −6 dB beam widths of these methods were 1.7, 1.0, 0.7, and 0.36 mm, respectively. The estimation errors of these methods in echo intensity were 0, 3.2, and 1.6 dB, respectively. The numbers of operations for the conventional method and the proposed method were 7800 and 532, respectively. The computational complexity of the proposed technique was less than 7% that of the conventional method.

To evaluate the calculation time required to make a 300 × 26 pixel image, we used a Linux workstation with an Intel® core-i7 CPU. The calculation times were 656 ms by the conventional BS Capon method and 81 ms by the proposed BS Capon method. The proposed method reduced the calculation time by 88% compared with the conventional BS Capon method. Because in the proposed method the intensity at each depth is calculated individually, we can
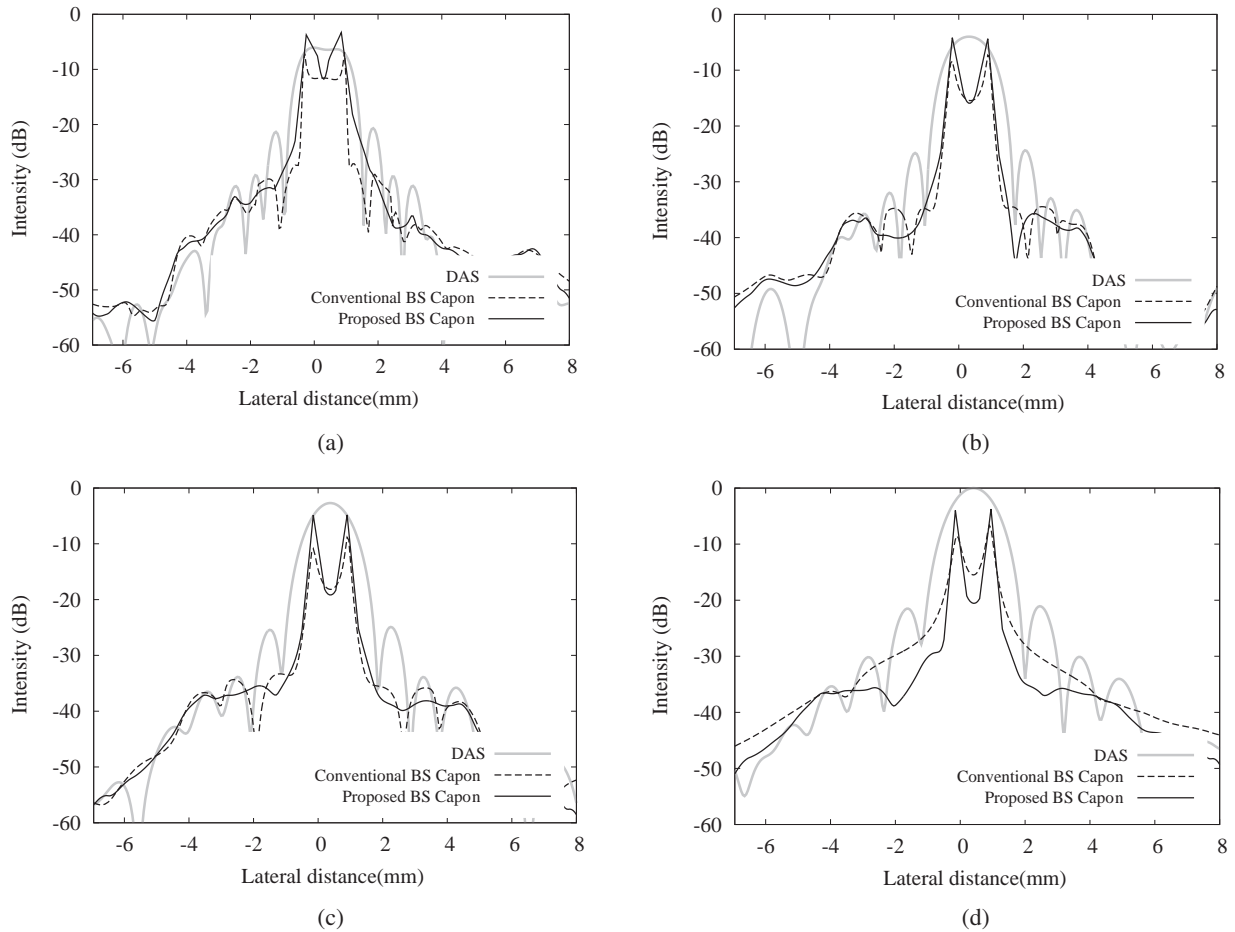
Fig. 5. Experimental result of cross-sectional images at the target depth obtained by the DAS method, the conventional BS Capon, and the proposed BS Capon method. The lateral interval of the targets was 1.0 mm and the target depths were (a) 21.4, (b) 31.4, (c) 41.4, and (d) 51.4 mm.

Table I. Experimental results of (a) the DAS method, (b) the conventional BS Capon method, and (c) the proposed BS Capon method. Each value is the average of four measurements at each depth.

	First side-lobe level (dB)	−6 dB beam width (mm)	Intensity estimation error (dB)	Number of operations	Calculation time (ms)
(a)	−5.3	1.7	0		
(b)	−15	0.7	3.2	7800	656
(c)	−17	0.36	1.6	532	81

Table II. Optimal weighting vector estimated by (a) the DAS method, (b) the conventional BS Capon method, and (c) the proposed BS Capon method at the depth of 40 mm and lateral distances of 0.5, 1.0, and 1.5 mm in the experimental study.

	Beam −1	Beam 0	Beam 1
Lateral distance of 0.5 mm			
(a)	0	0.13	0
(b)	$-0.33 + 0.010j$	0.13	$-0.47 + 0.080j$
(c)	$-0.47 + 0.2j$	$0.20 + 0.82j$	$-0.77 + 0.44j$
Lateral distance of 1.0 mm			
(a)	0	0.13	0
(b)	$-0.098 + 0.035j$	0.13	$-1.5 + 0.023j$
(c)	$-0.098 + 0.035j$	0.13	$-1.5 + 0.023j$
Lateral distance of 1.5 mm			
(a)	0	0.13	0
(b)	$0.0095 - 0.0018j$	0.13	$-0.41 - 0.17j$
(c)	$0.037 + 0.011j$	$0.053 - 0.047j$	$-0.17 + 0.0010j$

employ parallel calculations. When we employ three CPUs, the proposed method yields an image at 37 frames/s for a 15×10.4 mm^2 ROI.

Table II shows the weighting vector, $\mathbf{w}_{BS}$, calculated by the DAS technique, the conventional BS Capon method, and the proposed method at the depth of 41.4 mm and the lateral distances of 0.5, 1.0, and 1.5 mm. The focal point of the proposed method was the 1.0 mm lateral distance. The conventional DAS technique had the same weighting vector at all measurement points. The proposed method yielded the same $\mathbf{w}_{BS}$ as the conventional BS Capon method at the 1.0 mm lateral distance because that was also the focal point. When the distance between the focal point and the measurement point increased, weighting vectors estimated with the two methods were completely different.

4. Discussion

The reduction in the number of processes associated with the time-delay and transformation from ES signal processing to BS signal processing is determined by the sub-ROI size. In this experiment, we used Δx of 0.05 mm and sub-ROI size of 2.25 mm, i.e., the sub-ROI size was 45 pixels. As shown in Sect. 2.2, the interval of the focal point was 15 pixels.

Theoretically, the number of operations in the proposed method might be almost 6.7% of that in the conventional method when we dismiss the recalculation process. Indeed, the number of processes in the proposed method is 6.8% of that in the conventional method even when we take into account of recalculation processes.

However, as shown in Sect. 4, the calculation times for the conventional method and the proposed method were 656 and 81 ms, respectively. The reduction in the calculation time is smaller than the expected reduction. Both conventional and proposed BS Capon methods require an analytic signal at each element. Thus, the RF signals must be transformed into analytic signals. The process is employed by both methods and the calculation time associated with the process is 32 ms. When we dismiss this calculation time, the calculation times for the conventional method and the proposed method are 624 and 50 ms, respectively. The proposed method reduced the calculation time by 92% of the whole calculation time under this situation.

The error caused by the approximation is small at deeper areas because the distance from the focal point to the measurement point $d_{r,m} - d_{x,m}$ for deep areas is smaller than that at shallow areas. The proposed method of using a large sub-ROI size may yield accurate images of deep areas. Further reduction in complexity may be possible by optimizing the sub-ROI size at each depth.

Theoretically, the imaging performance of the proposed method without power compensation is almost the same as that of the conventional BS Capon method when we use the same subarray size for both methods. As shown in Table I, the proposed method improves the first side-lobe level and beam width. These improvements were brought about by the power compensation technique.

5. Conclusions

In this paper, we proposed techniques that reduce the computational complexity of medical ultrasound imaging by the BS Capon method. A reduction in the number of time-delay processes and a transformation from ES to BS signal processing were required. We replaced the time-delay process by the multiplication of a steering vector and a covariance matrix to reduce the number of processes. Additionally, to achieve accurate echo intensity estimation, we employed a compensation technique of using a small subarray size.

In an experimental study using a 2.0 MHz center frequency, the proposed method successfully depicted two closely positioned targets with a lateral interval of 1.0 mm. In the proposed method, the number of processes was reduced from 7800 to 532, the first side-lobe level was suppressed from -15 to -17 dB, and the estimation error in echo intensity was decreased from 3.2 to 1.6 dB. The calculation time required for generating a 300×26 pixel image by the proposed method was 81 ms, which is less than 13% of the time required in the case of the conventional BS Capon method. By the proposed method and parallel processing on three CPUs, 37 frames/s imaging was achieved. These results indicate that the proposed method may have the potential to implement adaptive signal processing for real-time medical ultrasound imaging.

1) H. Isono, S. Hirata, and H. Hachiya, Jpn. J. Appl. Phys. **54**, 07HF15 (2015).
2) Y. Miyachi, H. Hasegawa, and H. Kanai, Jpn. J. Appl. Phys. **54**, 07HF18 (2015).
3) L. Liu, S. Yagi, and H. Bian, Jpn. J. Appl. Phys. **54**, 07HF17 (2015).
4) S. Mori, S. Hirata, T. Yamaguchi, and H. Hachiya, Jpn. J. Appl. Phys. **54**, 07HF20 (2015).
5) T. Higuchi, S. Hirata, T. Yamaguchi, and H. Hachiya, Jpn. J. Appl. Phys. **53**, 07KF27 (2014).
6) S. Mori, S. Hirata, and H. Hachiya, Jpn. J. Appl. Phys. **53**, 07KF23 (2014).
7) H. Hasegawa and H. Kanai, Jpn. J. Appl. Phys. **53**, 07KF02 (2014).
8) T. Yamamura, M. Tanabe, K. Okubo, and N. Tagawa, Jpn. J. Appl. Phys. **51**, 07GF01 (2012).
9) H. Taki, M. Yamakawa, T. Shiina, and T. Sato, Jpn. J. Appl. Phys. **54**, 07HF03 (2015).
10) A. Ponnle, H. Hasegawa, and H. Kanai, Jpn. J. Appl. Phys. **50**, 07HF05 (2011).
11) C. C. Nilsen and I. Hafizovic, IEEE Trans. Ultrason. Ferroelectr. Freq. Control **56**, 2187 (2009).
12) S. Okumura, H. Taki, and T. Sato, Proc. IEEE EMBC, 2015, p. 6334.
13) S. Okumura, H. Taki, and T. Sato, Proc. IEEE ICASSP, 2015, p. 892.
14) J.-F. Synnevåg, A. Austeng, and S. Holm, IEEE Trans. Ultrason. Ferroelectr. Freq. Control **56**, 1868 (2009).
15) S. Mehdizadeh, A. Austeng, T. F. Johansen, and S. Holm, IEEE Trans. Ultrason. Ferroelectr. Freq. Control **59**, 683 (2012).
16) Z. Wang, J. Li, and R. Wu, IEEE Trans. Med. Imaging **24**, 1308 (2005).
17) H. Hasegawa and H. Kanai, IEEE Trans. Ultrason. Ferroelectr. Freq. Control **62**, 511 (2015).
18) A. C. Jensen and A. Austeng, IEEE Trans. Ultrason. Ferroelectr. Freq. Control **59**, 1139 (2012).
19) H. Taki, T. Sakamoto, M. Yamakawa, T. Shiina, T. Sato, K. Taki, and M. Kudo, Proc. IEEE Ultrasonics Symp., 2013, p. 805.
20) H. Taki, K. Taki, M. Yamakawa, T. Shiina, M. Kudo, and T. Sato, Jpn. J. Appl. Phys. **54**, 07HF05 (2015).
21) T. Kimura, H. Taki, T. Sakamoto, and T. Sato, Jpn. J. Appl. Phys. **48**, 07GJ07 (2009).
22) H. Taki, Y. Nagatani, M. Matsukawa, K. Mizuno, and T. Sato, J. Acoust. Soc. Am. **137**, 1683 (2015).
23) H. Taki, K. Taki, T. Sakamoto, M. Yamakawa, T. Shiina, M. Kudo, and T. Sato, IEEE Trans. Med. Imaging **31**, 417 (2012).
24) J. Capon, Proc. IEEE **57**, 1408 (1969).
25) K. Takao and N. Kikuma, IEEE Trans. Antennas Propag. **35**, 1389 (1987).
26) J. A. Jensen, Med. Biol. Eng. Comput. **34**, [Suppl. 1, Part 1], 351 (1996).
27) J. A. Jensen and N. B. Svendsen, IEEE Trans. Ultrason. Ferroelectr. Freq. Control **39**, 262 (1992).
28) H. Taki, S. Tanimura, T. Sakamoto, T. Shiina, and T. Sato, J. Med. Ultrason. **42**, 51 (2015).
29) J. A. Jensen, S. I. Nikolov, K. L. Gammelmark, and M. H. Pedersen, Ultrasonics **44**, e5 (2006).
30) H. Takahashi, H. Hasegawa, and H. Kanai, Jpn. J. Appl. Phys. **53**, 07KF08 (2014).
31) H. Hasegawa and H. Kanai, IEEE Trans. Ultrason. Ferroelectr. Freq. Control **59**, 2569 (2012).